



TECH BRIEFS

NATIONAL AERONAUTICS AND SPACE ADMINISTRATION

-  **Technology Focus**
-  **Electronics/Computers**
-  **Software**
-  **Materials**
-  **Mechanics/Machinery**
-  **Manufacturing**
-  **Bio-Medical**
-  **Physical Sciences**
-  **Information Sciences**
-  **Books and Reports**

INTRODUCTION

Tech Briefs are short announcements of innovations originating from research and development activities of the National Aeronautics and Space Administration. They emphasize information considered likely to be transferable across industrial, regional, or disciplinary lines and are issued to encourage commercial application.

Availability of NASA Tech Briefs and TSPs

Requests for individual Tech Briefs or for Technical Support Packages (TSPs) announced herein should be addressed to

National Technology Transfer Center

Telephone No. (800) 678-6882 or via World Wide Web at www.nttc.edu

Please reference the control numbers appearing at the end of each Tech Brief. Information on NASA's Innovative Partnerships Program (IPP), its documents, and services is also available at the same facility or on the World Wide Web at <http://www.nasa.gov/offices/ipp/network/index.html>

Innovative Partnerships Offices are located at NASA field centers to provide technology-transfer access to industrial users. Inquiries can be made by contacting NASA field centers listed below.

Ames Research Center

Lisa L. Lockyer
(650) 604-1754
lisa.l.lockyer@nasa.gov

Dryden Flight Research Center

Gregory Poteat
(661) 276-3872
greg.poteat@dfrc.nasa.gov

Glenn Research Center

Kathy Needham
(216) 433-2802
kathleen.k.needham@nasa.gov

Goddard Space Flight Center

Nona Cheeks
(301) 286-5810
nona.k.cheeks@nasa.gov

Jet Propulsion Laboratory

Andrew Gray
(818) 354-3821
gray@jpl.nasa.gov

Johnson Space Center

information
(281) 483-3809
jsc.techtran@mail.nasa.gov

Kennedy Space Center

David R. Makufka
(321) 867-6227
david.r.makufka@nasa.gov

Langley Research Center

Brian Beaton
(757) 864-2192
brian.f.beaton@nasa.gov

Marshall Space Flight Center

Jim Dowdy
(256) 544-7604
jim.dowdy@msfc.nasa.gov

Stennis Space Center

Ramona Travis
(228) 688-3832
ramona.e.travis@nasa.gov

Carl Ray, Program Executive

Small Business Innovation
Research (SBIR) & Small
Business Technology
Transfer (STTR) Programs
(202) 358-4652
carl.g.ray@nasa.gov

Doug Comstock, Director

Innovative Partnerships
Program Office
(202) 358-2560
doug.comstock@nasa.gov



TECH BRIEFS

NATIONAL AERONAUTICS AND SPACE ADMINISTRATION



5 Technology Focus: Data Acquisition

- 5 A Deep Space Network Portable Radio Science Receiver
- 5 Detecting Phase Boundaries in Hard-Sphere Suspensions
- 6 Low-Complexity Lossless and Near-Lossless Data Compression Technique for Multispectral Imagery
- 7 Very-Long-Distance Remote Hearing and Vibrometry
- 7 Using GPS to Detect Imminent Tsunamis
- 8 Stream Flow Prediction by Remote Sensing and Genetic Programming



9 Electronics/Computers

- 9 Pilotless Frame Synchronization Using LDPC Code Constraints
- 10 Radiometer on a Chip
- 10 Measuring Luminescence Lifetime With Help of a DSP
- 10 Modulation Based on Probability Density Functions
- 11 Ku Telemetry Modulator for Suborbital Vehicles
- 11 Photonic Links for High-Performance Arraying of Antennas
- 13 Reconfigurable, Bi-Directional Flexfet Level Shifter for Low-Power, Rad-Hard Integration
- 13 Hardware-Efficient Monitoring of I/O Signals
- 13 Video System for Viewing From a Remote or Windowless Cockpit
- 14 Spacesuit Data Display and Management System
- 14 IEEE 1394 Hub With Fault Containment
- 14 Compact, Miniature MMIC Receiver Modules for an MMIC Array Spectrograph
- 15 Waveguide Transition for Submillimeter-Wave MMICs
- 15 Magnetic-Field-Tunable Superconducting Rectifier



17 Manufacturing & Prototyping

- 17 Bonded Invar Clip Removal Using Foil Heaters
- 17 Fabricating Radial Groove Gratings Using Projection Photolithography

- 17 Gratings Fabricated on Flat Surfaces and Reproduced on Non-Flat Substrates



19 Physical Sciences

- 19 Method for Measuring the Volume-Scattering Function of Water
- 19 Method of Heating a Foam-Based Catalyst Bed
- 19 Small Deflection Energy Analyzer for Energy and Angular Distributions
- 20 Polymeric Bladder for Storing Liquid Oxygen
- 20 Pyrotechnic Simulator/Stray-Voltage Detector
- 20 Inventions Utilizing Microfluidics and Colloidal Particles
- 21 RuO₂ Thermometer for Ultra-Low Temperatures
- 21 Ultra-Compact, High-Resolution LADAR System for 3D Imaging
- 21 Dual-Channel Multi-Purpose Telescope
- 22 Objective Lens Optimized for Wavefront Delivery, Pupil Imaging, and Pupil Ghosting
- 22 CMOS Camera Array With Onboard Memory



23 Information Sciences

- 23 Quickly Approximating the Distance Between Two Objects
- 23 Processing Images of Craters for Spacecraft Navigation
- 23 Adaptive Morphological Feature-Based Object Classifier for a Color Imaging System
- 24 Rover Slip Validation and Prediction Algorithm
- 24 Safety and Quality Training Simulator
- 25 Supply-Chain Optimization Template
- 25 Algorithm for Computing Particle/Surface Interactions



27 Books & Reports

- 27 Cryogenic Pupil Alignment Test Architecture for Aberrated Pupil Images
- 27 Thermal Transport Model for Heat Sink Design

This document was prepared under the sponsorship of the National Aeronautics and Space Administration. Neither the United States Government nor any person acting on behalf of the United States Government assumes any liability resulting from the use of the information contained in this document, or warrants that such use will be free from privately owned rights.



A Deep Space Network Portable Radio Science Receiver

Receiver filters and records IF analog signals.

NASA's Jet Propulsion Laboratory, Pasadena, California

The Radio Science Receiver (RSR) is an open-loop receiver installed in NASA's Deep Space Network (DSN), which digitally filters and records intermediate-frequency (IF) analog signals. The RSR is an important tool for the Cassini Project, which uses it to measure perturbations of the radio-frequency wave as it travels between the spacecraft and the ground stations, allowing highly detailed study of the composition of the rings, atmosphere, and surface of Saturn and its satellites. The RSR is also used to track and detect the signals for important events in other missions such as the Mars Exploration Rover (MER) entry descent and landing (EDL). Some of these events require extra RSRs or require them to be shipped to non-DSN stations such as the 100-meter Greenbank Telescope (GBT) in West Virginia. Sending and installing an RSR consisting of a large DSN rack to one of these sites is a daunting and expensive task. A smaller, more portable equivalent to the RSR was needed both for these special events and to enhance the existing capability of the DSN.

A prototype Portable Radio Science Receiver (PRSR) has been developed that can fit in a standard-size suitcase and uses a laptop PC as its controlling computer. The PRSR chassis is a 2-U steel box with 19-in. (48-cm) rack-mount capability and external connections for power, Ethernet, RS-232 control, 100 MHz reference signal, 1-pulse-per-second reference, and one input port for an IF signal in the range of 0–640 MHz. Inside the PRSR, there is a steel plate that separates the IF digitizer unit from the digital signal-processing board to reduce spurs that may affect the sensitive analog components.

This innovation contains firmware that runs on a Xilinx field-programmable gate array (FPGA), and consists of code that down-converts the DSN's 640-MHz IF spectrum into two channels: a wide bandwidth channel and a narrow bandwidth channel. The wide bandwidth channel can be configured from 160 MHz down to 1.25 MHz with 16 bits of resolution. The narrow channel can be configured from 1.25 MHz down to 10 kHz with 32 bits of resolution.

The present PRSR software consists of a driver, a command processor, and a graphical user interface (GUI) for viewing monitor data and plots. While limited in scope, this software is able to demonstrate on the prototype hardware the key features of a fully operational PRSR. For example, data can be recorded onto a disk from the PRSR's narrowband channel, but recordings only occur in discontinuous snapshots of 4,096 samples each.

The PRSR was shipped to GBT along with an existing DSN RSR rack and recorded signals in parallel with the RSR coming from the Phoenix lander during the May 25, 2008 EDL. This test demonstrated the potential of the PRSR prototype and the value for developing it into a fully operational DSN receiver.

This work was done by Andre P. Jongeling, Elliott H. Sigman, Kumar Chandra, Joseph T. Trinh, Robert Navarro, Stephen P. Rogstad, Charles E. Goodhart, Robert C. Proctor, Susan G. Finley, and Leslie A. White of Caltech for NASA's Jet Propulsion Laboratory. For more information, contact iaoffice@jpl.nasa.gov. NPO-46289

Detecting Phase Boundaries in Hard-Sphere Suspensions

Liquid and solid phases are distinguished through differences in motions of spheres.

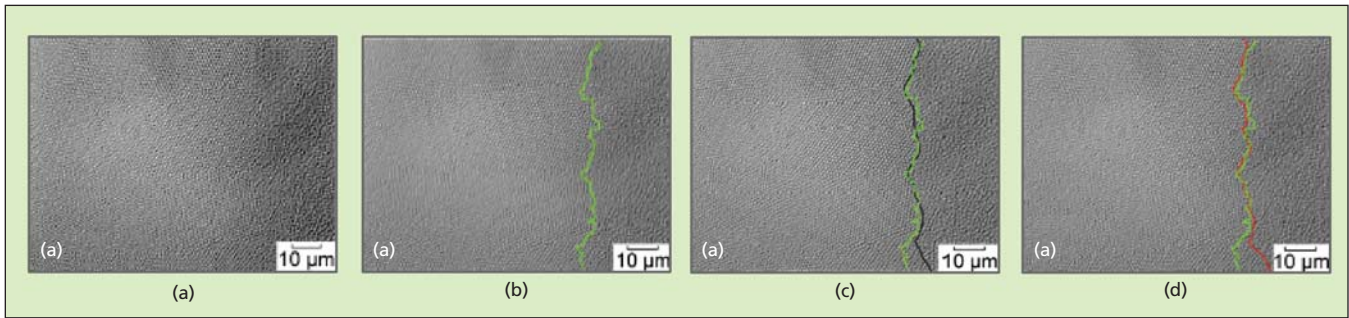
John H. Glenn Research Center, Cleveland, Ohio

A special image-data-processing technique has been developed for use in experiments that involve observation, via optical microscopes equipped with electronic cameras, of moving boundaries between the colloidal-solid and colloidal-liquid phases of colloidal suspensions of monodisperse hard spheres. Such suspensions are used as physical models of thermodynamic phase transitions and of precursors to photonic-band-gap materials. During an experiment, it is necessary to adjust the position of a microscope to keep the phase boundary within view. A boundary typically moves at a speed of

the order of microns per hour. Because an experiment can last days or even weeks, it is impractical to require human intervention to keep the phase boundary in view. The present image-data-processing technique yields results within a computation time short enough to enable generation of automated-microscope-positioning commands to track the moving phase boundary.

The experiments that prompted the development of the present technique include a colloidal equivalent of directional solidification. The interactions between the spheres in these suspensions

closely approximate an ideal hard-sphere potential, so that the phase behavior becomes, to a close approximation, solely a function of volume fraction (ϕ) of spheres. When ϕ of a given suspension sample is less than a threshold value ($\phi_f = 0.494$) denoted the freezing volume fraction, the suspension is in the colloidal-liquid phase, in which the spheres are disordered and free to diffuse throughout the entire volume of the sample. When ϕ exceeds another threshold value ($\phi_m = 0.545$) denoted the melting volume fraction, the suspension is in the colloidal-solid phase, in which the sample is crystalline in the



This **Image Sequence** illustrates the technique: (a) 1st image in the experiment sequence, (b) 1st automated interface technique ($n=10$) result superimposed on original image, (c) 1st automated interface technique ($n=10$) and authors' results superimposed on original image, and (d) 1st automated interface technique ($n=10$) and independent experts' results superimposed on original image.

sense that each sphere is “caged” by its neighbors and thus restricted to small movement about a lattice point. Between ϕ_f and ϕ_m is a regime of coexisting colloidal liquid and colloidal solid.

At the beginning of an experiment, a suspension is prepared at ϕ well below ϕ_f and placed in a cell. Then through slow evaporation or gravitational sedimentation, the spheres become concentrated toward one end of the cell, where crystallization starts when ϕ_f is reached. When the sphere size falls within a range accessible to optical microscopy, the disordered (liquid) phase and the ordered (solid) phase (and, hence, the boundary between them) are visible to, and clearly distinguishable by, a human observer. However, prior image-data-processing

techniques do not enable automated distinction between regions of order and disorder in images of closely packed spheres.

In the present technique, automated distinction (see figure) is made possible by differences between the motions of the spheres in the liquid and solid regions. In particular, the technique exploits the fact that in the solid phase, the spheres are restricted to their small “cages,” whereas in the liquid phase, the spheres are free to move. Consequently, when images are averaged over successive frame periods, the liquid region tends to become blurred or gray while the solid region retains a higher degree of contrast, showing the spheres as individual particles. Each frame-averaged image is subjected to a brightness-

slicing, a cleaning (noise-suppression), and a particle-finding operation. These operations utilize the brightness and contrast differences between the solid and liquid regions. Then the image region showing particles is deemed to be the solid region and the phase boundary is located accordingly.

This work was done by Mark McDowell and Richard B. Rogers of Glenn Research Center and Elizabeth Gray of Scientific Consulting, Inc. Further information is contained in a TSP (see page 1).

Inquiries concerning rights for the commercial use of this invention should be addressed to NASA Glenn Research Center, Innovative Partnerships Office, Attn: Steve Fedor, Mail Stop 4-8, 21000 Brookpark Road, Cleveland, Ohio 44135. Refer to LEW-18157-1.

Low-Complexity Lossless and Near-Lossless Data Compression Technique for Multispectral Imagery

The technique allows substantially smaller compressed file sizes when a small amount of distortion can be tolerated.

NASA's Jet Propulsion Laboratory, Pasadena, California

This work extends the lossless data compression technique described in “Fast Lossless Compression of Multispectral-Image Data,” (NPO-42517) *NASA Tech Briefs*, Vol. 30, No. 8 (August 2006), page 26. The original technique was extended to include a near-lossless compression option, allowing substantially smaller compressed file sizes when a small amount of distortion can be tolerated. Near-lossless compression is obtained by including a quantization step prior to encoding of prediction residuals.

The original technique uses lossless predictive compression and is designed for use on multispectral imagery. A lossless predictive data compression algo-

rithm compresses a digitized signal one sample at a time as follows: First, a sample value is predicted from previously encoded samples. The difference between the actual sample value and the prediction is called the prediction residual. The prediction residual is encoded into the compressed file. The decompressor can form the same predicted sample and can decode the prediction residual from the compressed file, and so can reconstruct the original sample.

A lossless predictive compression algorithm can generally be converted to a near-lossless compression algorithm by quantizing the prediction residuals prior to encoding them. In this case, since the reconstructed sample values will not be

identical to the original sample values, the encoder must determine the values that will be reconstructed and use these values for predicting later sample values. The technique described here uses this method, starting with the original technique, to allow near-lossless compression.

The extension to allow near-lossless compression adds the ability to achieve much more compression when small amounts of distortion are tolerable, while retaining the low complexity and good overall compression effectiveness of the original algorithm.

This work was done by Hua Xie and Matthew A. Klimesh of Caltech for NASA's Jet Propulsion Laboratory. For more information, contact iaoffice@jpl.nasa.gov. NPO-46625

Very-Long-Distance Remote Hearing and Vibrometry

Optical returns from weakly illuminated targets would be processed by advanced techniques.

NASA's Jet Propulsion Laboratory, Pasadena, California

A proposed development of laser-based instrumentation systems would extend the art of laser Doppler vibrometry beyond the prior limits of laser-assisted remote hearing and industrial vibrometry for detecting defects in operating mechanisms. A system according to the proposal could covertly measure vibrations of objects at distances as large as thousands of kilometers and could process the measurement data to enable recognition of vibrations characteristic of specific objects of interest, thereby enabling recognition of the objects themselves. A typical system as envisioned would be placed in orbit around the Earth for use as a means of determining whether certain objects on or under the ground are of interest as potential military targets. Terrestrial versions of these instruments designed for airborne or land- or sea-based operation could be similarly useful for military or law-enforcement purposes.

Prior laser-based remote-hearing systems are not capable of either covert operation or detecting signals beyond modest distances when operated at realistic laser power levels. The performances of prior systems for recognition of objects by remote vibrometry are limited by low signal-to-noise ratios and lack of filtering of optical signals returned from targets. The proposed development would overcome these limitations.

A system as proposed would include a narrow-band laser as its target illuminator, a lock-in-detection receiver subsystem, and a laser-power-control subsystem that would utilize feedback of the intensity of background illumination of the target to adjust the laser power. The laser power would be set at a level high enough to enable the desired measurements but below the threshold of detectability by an imaginary typical modern photodetector located at the target and there exposed to the background illumination. The laser beam would be focused tightly on the distant target, such that the receiving optics would be exposed to only one speckle. The return signal would be extremely-narrow-band filtered (to sub-kilohertz bandwidth) in the optical domain by a whispering-gallery-mode filter so as to remove most of the background illumination. The filtered optical signal would be optically amplified. This combination of optical filtering and optical amplification would provide an optical signal that would be strong enough to be detectable but not so strong as to saturate the detector in the lock-in detection subsystem.

The laser emission would be modulated by an optical modulator driven by a low-frequency oscillator. The same oscillator would drive a lock-in amplifier in the lock-in-detection receiver subsystem. It has been estimated that the lock-in

amplification would contribute 30 dB to the signal-to-noise ratio.

It has been estimated that a system of this type operating at a laser power of 0.2 W could enable recognition of an object at a distance of 1,000 miles ($\approx 1,600$ km). Examples of objects of potential military significance that could be recognized include particular machines shielded under the roof of a factory or deep underground, fake garages or factories, fake weapons, land mines, and improvised explosive devices. Vibrations induced by nearby motorized vehicles are expected to be sufficient to enable recognition of buried land mines.

This work was done by Lute Maleki, Nan Yu, Andrey Matsko, and Anatoliy Savchenkov of Caltech for NASA's Jet Propulsion Laboratory. Further information is contained in a TSP (see page 1).

In accordance with Public Law 96-517, the contractor has elected to retain title to this invention. Inquiries concerning rights for its commercial use should be addressed to:

*Innovative Technology Assets Management
JPL*

Mail Stop 202-233

4800 Oak Grove Drive

Pasadena, CA 91109-8099

E-mail: iaoffice@jpl.nasa.gov

Refer to NPO-45309, volume and number of this NASA Tech Briefs issue, and the page number.

Using GPS to Detect Imminent Tsunamis

Reliable tsunami warnings could be generated within minutes of causative earthquakes.

NASA's Jet Propulsion Laboratory, Pasadena, California

A promising method of detecting imminent tsunamis and estimating their destructive potential involves the use of Global Positioning System (GPS) data in addition to seismic data. Application of the method is expected to increase the reliability of global tsunami-warning systems, making it possible to save lives while reducing the incidence of false alarms.

Tsunamis kill people every year. The 2004 Indian Ocean tsunami killed about 230,000 people. The magnitude of an earthquake is not always a reliable indication of the destructive potential of a

tsunami. The 2004 Indian Ocean quake generated a huge tsunami, while the 2005 Nias (Indonesia) quake did not, even though both were initially estimated to be of the similar magnitude. Between 2005 and 2007, five false tsunami alarms were issued worldwide. Such alarms result in negative societal and economic effects.

GPS stations can detect ground motions of earthquakes in real time, as frequently as every few seconds. In the present method, the epicenter of an earthquake is located by use of data from seismometers, then data from

coastal GPS stations near the epicenter are used to infer sea-floor displacements that precede a tsunami. The displacement data are used in conjunction with local topographical data and an advanced theory to quantify the destructive potential of a tsunami on a new "tsunami scale," based on the GPS-derived tsunami energy, much like the Richter Scale used for earthquakes. An important element of the derivation of the advanced theory was recognition that horizontal sea-floor motions contribute much more to generation of

tsunamis than previously believed. The method produces a reliable estimate of the destructive potential of a tsunami within minutes — typically, well before the tsunami reaches coastal areas.

The viability of the method was demonstrated in computational tests in which the method yielded accurate rep-

resentations of three historical tsunamis for which well-documented ground-motion measurements were available. Development of a global tsunami-warning system utilizing an expanded network of coastal GPS stations was under consideration at the time of reporting the information for this article.

This work was done by Y. Tony Song of Caltech for NASA's Jet Propulsion Laboratory.

The software used in this innovation is available for commercial licensing. Please contact Karina Edmonds of the California Institute of Technology at (626) 395-2322. Refer to NPO-45940.

Stream Flow Prediction by Remote Sensing and Genetic Programming

A genetic programming model assimilates SAR images and geoenvironmental parameters to assess soil moisture at the watershed scale.

Stennis Space Center, Mississippi

A genetic programming (GP)-based, nonlinear modeling structure relates soil moisture with synthetic-aperture-radar (SAR) images to present representative soil moisture estimates at the watershed scale. Surface soil moisture measurement is difficult to obtain over a large area due to a variety of soil permeability values and soil textures. Point measurements can be used on a small-scale area, but it is impossible to acquire such information effectively in large-scale watersheds. This model exhibits the capacity to assimilate SAR images and relevant geoenvironmental parameters to measure soil moisture.

In the past, spaceborne radar imaging satellites used all-weather observation, but estimation methods of soil moisture based on active or passive satellite images remains uncertain. Estimation of soil moisture based on SAR measurement was made possible by developing linear re-

gression models and nonlinear regression models in a single land use/land cover from several hundred square meters to several square kilometers, based on traditional statistical regression theory. This GP-based artificial intelligence mode uses an evolutionary computational approach to estimate soil moisture with a variety of land use/land cover patterns.

The function derived in the evolutionary computation links a series of crucial topographical and geographical features including slope, aspect, vegetation cover, and soil permeability with well-calibrated SAR data. Research findings indicate that this development and application of the GP model has proved useful for generating a highly nonlinear structure in regression regimes, which exhibit strong statistical correlations between the model estimates and the ground truth measurements (volumetric water content), based on unseen datasets.

Using this model, science missions would be capable of handling large-scale moisture estimation using spaceborne satellite images, and could generate multi-temporal soil moisture maps over seasons. The GP-model is ultimately extensible and interoperable for any river basin of interest, though the impact of landscape complexity needs to be studied further.

This work was done by Ni-Bin Chang of Texas A&M University for Stennis Space Center.

Inquiries concerning rights for its commercial use should be addressed to:

*Texas A&M University
332 Wisenbacker Eng. Research Center
College Station, TX 77843-3000
Phone No.: (407) 823-1375
E-mail: nchang@mail.ucf.edu*

Refer to SSC-00256, volume and number of this NASA Tech Briefs issue, and the page number.



Pilotless Frame Synchronization Using LDPC Code Constraints

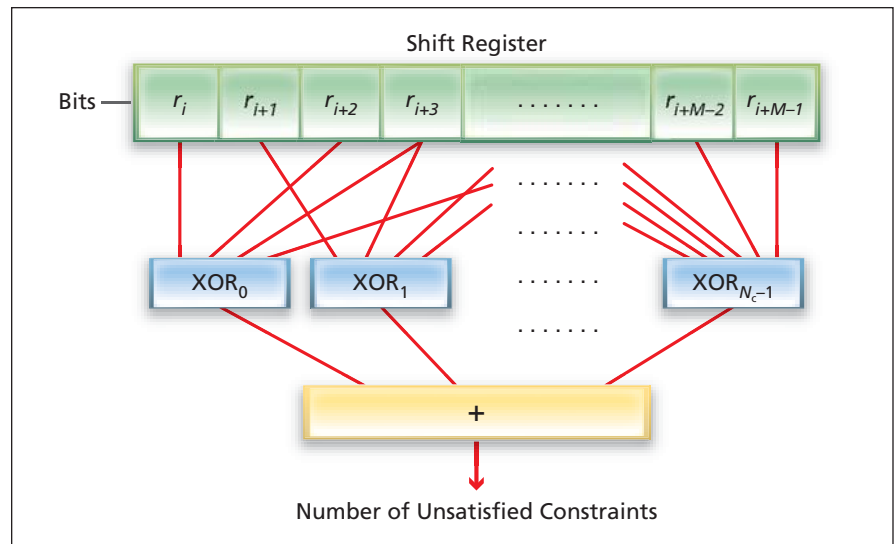
Performance equals or exceeds that attainable by use of pilot symbols.

NASA's Jet Propulsion Laboratory, Pasadena, California

A method of pilotless frame synchronization has been devised for low-density parity-check (LDPC) codes. Heretofore, it has been conventional practice to add pilot symbols, which serve as frame-synchronization markers, to LDPC codes as well as to some other codes. The reception of a signal modulated by a code accompanied by pilot symbols includes a process, separate from the decoding process, in which a correlation rule is used to estimate an offset between (1) the actual received code frame time and (2) a previous estimate of the code frame time. The estimate of the offset then serves as feedback for correcting the previous estimate of the frame time. On the other hand, in pilotless frame synchronization, there are no pilot symbols; instead, the offset is estimated by exploiting selected aspects of the structure of the code. The advantage of pilotless frame synchronization is that the bandwidth of the signal is reduced by an amount associated with elimination of the pilot symbols. The disadvantage is an increase in the amount of receiver data processing needed for frame synchronization.

The present method of pilotless frame synchronization is an instance of code-aided frame synchronization. Most of the prior research on code-aided frame synchronization has focused on Viterbi and turbo codes. One prior method applicable to an LDPC code involves performance of an LDPC iteration and monitoring of the mean of the absolute values of log-likelihood ratios (LLRs) of the variable nodes of the code. The rationale for this method is that the said mean values should be higher for correctly temporally aligned than for incorrectly temporally aligned code words. While this prior method is effective as a means of synchronization, it requires performance of a full LDPC iteration for every possible candidate offset.

The present method of pilotless frame synchronization does not require full LDPC iterations. Instead, it involves exploitation of information available from the constraint nodes of the LDPC code. In an LDPC code, a constraint node rep-



The **Number of Unsatisfied Constraints** can be computed by using the hardware functional blocks shown here. The labels (r_i, r_{i+1}, \dots) represent bits embodying a decision concerning a decoded symbol. N_c represents the total number of constraints. M represents the number of variable nodes (or block length).

resents a parity-check equation in which a set of variable nodes is used as a set of inputs. A valid decoded code word is deemed to be obtained if all parity-check equations are satisfied. Heretofore normally, the information from constraint nodes has been utilized only within the iterative LDPC decoding process to assess the convergence behavior of the process. However, the constraint-node information also has value for frame synchronization in that the number and nature of satisfied constraint-node equations serve as a measure, not only of code convergence, but also of the accuracy of estimates of frame-time offsets.

In the present method, hard decisions concerning received symbols are used in the parity-check computations for each constraint node. Because these computations consist mostly of exclusive-OR (XOR) operations, they are considerably less complex than are those of full LDPC iterations. The method could be implemented in hardware that would include a shift register, a multi-operand XOR block for each constraint node, and a multi-operand adder (see figure). The output of the adder — the number

of unsatisfied constraints — would be subtracted from the total number of constraints to obtain the number of satisfied constraints.

The present method of pilotless frame synchronization, and alternative methods of synchronization by use of pilot symbols, have been tested by means of computational simulations on a representative LDPC code. Comparative analysis of the results of the simulations has led to the conclusion that the present method of pilotless frame synchronization yields equal or superior performance in the sense that the signal-to-noise ratio needed to keep the bit-error rate from exceeding a given value in this method can be equal to or lower than that needed in any of the alternative methods.

This work was done by Christopher Jones of Caltech and Dong-U Lee, Hyungjin Kim, and John Villasenor of the UCLA Electrical Engineering Department for NASA's Jet Propulsion Laboratory.

The software used in this innovation is available for commercial licensing. Please contact Karina Edmonds of the California Institute of Technology at (626) 395-2322. Refer to NPO-45032.

Radiometer on a Chip

NASA's Jet Propulsion Laboratory, Pasadena, California

Submillimeter-wave radiometers have traditionally been built by packaging each chip with a distinct function separately, and then combining the packaged chips to form subsystems. Instead of packaging one chip at a time, the radiometer on a chip (ROC) integrates whole wafers together to provide a robust, extremely powerful way of making submillimeter receivers that provide vertically integrated functionality. By integrating at the wafer level, customizing the interconnects, and planarizing the transmission media, it is possible to create a lightweight assembly performing

the function of several pieces in a more conventional radiometer. This represents a greater than 50-fold decrease in both volume and mass. The act of combining the individual radiometer functions into a sequence of chips will also improve inter-component matching and reduce the loss associated with the power combining that accompanies today's radiometers.

Most of the gain fluctuations in present-day radiometers are the result of thermal gradients. By reducing the size and mass of the radiometer, the thermal gradients are reduced, thus also reduc-

ing their effect on thermal stability. This results in greater measurement stability.

With a size reduction of this magnitude, ROCs will be able to be used in balloons, landers, rovers, and any other place where a complete remote chemical laboratory might be required.

This work was done by Goutam Chattopadhyay, John J. Gill, Imran Mehdi, Choonsup Lee, Erich T. Schlecht, Anders Skalare, John S. Ward, Peter H. Siegel, and Bertrand C. Thomas of Caltech for NASA's Jet Propulsion Laboratory. For more information, contact iaoffice@jpl.nasa.gov. NPO-46542

Measuring Luminescence Lifetime With Help of a DSP

Lyndon B. Johnson Space Center, Houston, Texas

An instrument for measuring the lifetime of luminescence (fluorescence or phosphorescence) includes a digital signal processor (DSP) as the primary means of control, generation of excitation signals, and analysis of response signals. In contrast, prior luminescence-lifetime-measuring instruments have utilized primarily analog circuitry to perform these functions. Such instruments are typically used as optical chemical sensors.

Like the prior instruments, the present instrument is based on the principle of illuminating a specimen with sinusoidally

varying light to excite sinusoidally varying luminescence and measuring either the phase shift (ϕ) between the luminescence oscillations and the excitation signal at a specified frequency (f) or the frequency that results in a specified fixed phase shift (typically, 90°). The fluorescence lifetime (τ) is then calculated using $\tau = \tan \phi / (2\pi f)$. The primary limitation of prior analog instruments was lack of reconfigurability: it was necessary to rewire components to change operating modes for different specimens. In contrast, the DSP hardware in the present instrument makes it possible to switch among a vari-

ety of operating modes by making changes in software only.

This work was done by J. D. S. Danielson of PhotoSense LLC for Johnson Space Center. Further information is contained in a TSP (see page 1).

In accordance with Public Law 96-517, the contractor has elected to retain title to this invention. Inquiries concerning rights for its commercial use should be addressed to:

PhotoSense LLC

PO Box 20687

Boulder, CO 80308-3687

Refer to MSC-22906-1, volume and number of this NASA Tech Briefs issue, and the page number.

Modulation Based on Probability Density Functions

This method would have steganographic value.

John H. Glenn Research Center, Cleveland, Ohio

A proposed method of modulating a sinusoidal carrier signal to convey digital information involves the use of histograms representing probability density functions (PDFs) that characterize samples of the signal waveform. Although almost any modulation can be characterized as amplitude, phase, or frequency modulation or some combination of two or all three of them, the proposed method is independent of traditional modes of amplitude, phase, and frequency modulation and neither

explicitly includes nor explicitly excludes them.

The method is based partly on the observation that when a waveform is sampled (whether by analog or digital means) over a time interval at least as long as one half cycle of the waveform, the samples can be sorted by frequency of occurrence, thereby constructing a histogram representing a PDF of the waveform during that time interval. Commonly known data-analysis and statistical techniques (e.g., those of pattern

recognition or correlation), implemented in software, can reveal a trend in the histogram associated with some aspect of the shape of the sampled segment of the waveform. In the proposed method, the waveform would be shaped, at the transmitter, such that the trend in the histogram to be generated at the receiver would encode a digital datum (e.g., a one or a zero in the case of binary encoding).

A receiver according to this method could be embodied in analog or digital

circuitry. In an analog embodiment, the histogram of the signal would be captured by a tree of window comparator/integrators, there being one branching level of the tree for each of n compartments of the histogram. The final analog calculation of the aspect of shape of the histogram that encodes the desired information would be performed by various hard-wired combinations of n -level summing amplifiers. A digital embodiment would include a single analog-to-digital converter operating at a sampling rate high enough to avoid aliasing. The PDF modulation would be detected by software that would examine the histogram table.

Regardless of the analog or digital nature of the receiver circuitry, the transmitter would best be embodied in a

combination of digital and analog circuitry: The waveform-shaping computations for encoding the information to be conveyed would be performed digitally. The resulting numbers would be fed as input to a digital-to-analog converter to generate the analog waveform to be amplified and used to generate the transmitted signal.

The main advantage of the method would lie in its value as the basis of an electronic form of steganography. Because a message would be encoded in statistical characteristics of a waveform, neither the existence nor the contents of the message could easily be discerned by simple inspection of the waveform.

Some types of PDF-modulation waveforms are expected to be resilient in the

presence of interference and jamming if properly used in digital-signal-processing radio-relay systems: examples include sawtooth and square waveforms. On the other hand, at low receiver signal-to-noise ratios, decoding can be problematic in cases in which users do not take care to select modulation waveforms that are easily recognizable in the presence of noise.

This work was done by Glenn L. Williams of Glenn Research Center. Further information is contained in a TSP (see page 1).

Inquiries concerning rights for the commercial use of this invention should be addressed to NASA Glenn Research Center, Innovative Partnerships Office, Attn: Steve Fedor, Mail Stop 4-8, 21000 Brookpark Road, Cleveland, Ohio 44135. Refer to LEW-17650-1.

Ku Telemetry Modulator for Suborbital Vehicles

Goddard Space Flight Center, Greenbelt, Maryland

A modulator utilizing the Ku-band instead of the usual S-band has been developed to improve transmission rates for suborbital platforms. The unit operates in the 14.5–15.5-GHz band and supports data rates up to 200 Mbps.

In order to keep the modulator costs low, the modulator is based on the LCT2 [Low Cost TDRSS (Tracking and Data Relay Satellite System)] Transceiver design, which utilizes a single-board modulator incorporating an Analog Devices quadrature modulator IC, with I&Q [in-phase (I) and quadrature (Q)] bandwidths of 70 MHz. A pin-compatible ver-

sion of the chips with I&Q bandwidths of up to 160 MHz is used to achieve the higher data rates. To support the higher data rate, an LVDS (low-voltage differential signaling) user interface will be incorporated into the modulator board. The LCT2 configuration uses a 1×4 in. (≈2.5×10.2 cm) high-power S-band amplifier module. The new amplifier printed circuit board (PCB) module is replaced with a compact S-band to Ku-band up-converter, with an RF output of +5 dBm.

A key feature is the unit's small form factor of 4×5×1.5 in. (≈10.2×12.7×3.8 cm). It has a low complexity, consisting

of two PCBs and a DC/DC converter. This keeps the cost down, which is an important feasibility issue for the types of missions that it is designed for — low-cost suborbital. This modulator is useful for any suborbital platform such as sounding rockets, balloons, unmanned aerial vehicles (UAVs), and expendable launch vehicles.

This work was done by Steven Bundick of Goddard Space Flight Center and Jim Bishop, David Newman, and Nazrul Zaki of LJT & Associates. For further information, contact the Goddard Innovative Partnerships Office at (301) 286-5810. GSC-15456-1

Photonic Links for High-Performance Arraying of Antennas

Advantages over RF arraying architecture would include reduced cost and increased reliability.

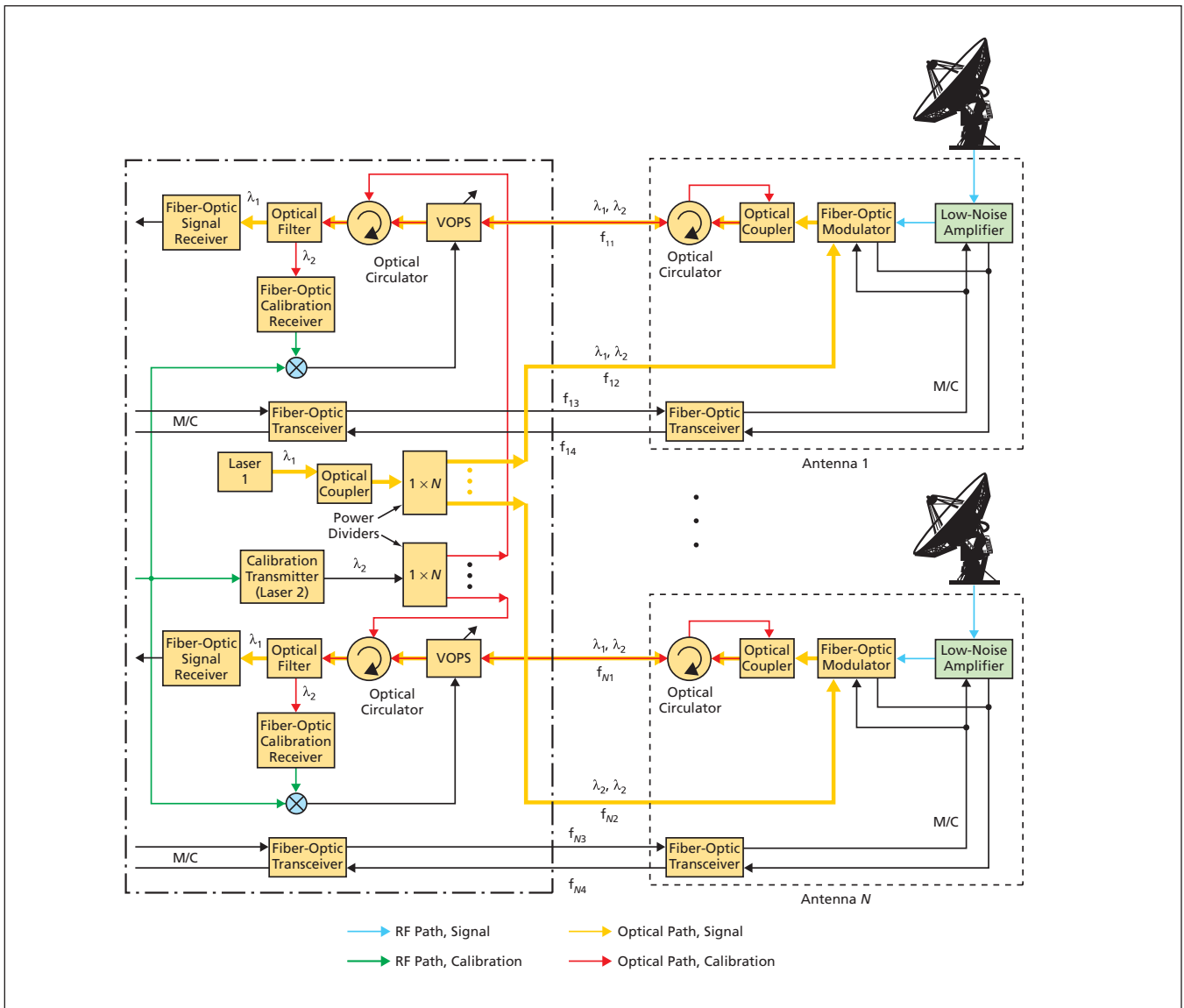
NASA's Jet Propulsion Laboratory, Pasadena, California

An architecture for arraying microwave antennas in the next generation of NASA's Deep Space Network (DSN) involves the use of all photonic links between (1) the antennas in a given array and (2) a signal-processing center. As used here, "arraying" refers generally to any or all of several functions that include control and synchronization functions; coherent combination of signals received by multiple antennas at different locations in such a way as to improve reception, as though one had a single larger antenna; and coherent

radiation of signals for transmission of an intense, narrow beam toward a distant spacecraft or other target. This all-photonic arraying architecture can also be adapted to arraying of radio antennas other than those of the DSN. In this architecture, all affected parts at each antenna pedestal [except a front-end low-noise amplifier for the radio-frequency (RF) signal coming from the antenna and an optical transceiver to handle monitor and control (M/C) signals] would be passive optical parts. Potential advantages of this all-pho-

tonic link architecture over the RF architecture now in use include cost savings, increased stability of operation, increased reliability, and a reduction in the time and materials expended in maintenance at each antenna.

A basic arraying system according to this architecture (see figure) would utilize only a single high-power laser (emitting at wavelength λ_1) and several lower-power lasers in the signal-processing center to drive fiber-optic links between the center and N antennas. In the future DSN appli-



The All-Photonic Arraying Architecture is depicted here in simplified form: For the sake of clarity in illustrating the underlying principles, such details as partly separate paths for handling X- and Ka-band RF signals are omitted.

As now envisioned, the lengths of the fiber-optic links would be of the order of a kilometer. The λ_1 laser signal would be split by a $1 \times N$ power divider then distributed to all N antennas in the array via optical fibers denoted in the figure as $f_{12} \dots f_{N2}$. At each antenna, the incoming λ_1 laser signal would be coupled into a fiber-optic modulator, which would be driven by an amplified version of the RF signal received by the antenna. The modulated λ_1 light would pass through an optical coupler and an optical circulator, from whence it would travel to the signal-processing center via optical fibers ($f_{11} \dots f_{N1}$). These aspects of the architecture eliminate the need for radio-frequency (RF) down-conversion, phased-locked-loop, and other equipment traditionally used at each antenna to process the signal(s) received by that antenna.

At the center, the incoming λ_1 signal light would pass through a variable optical phase shifter (VOPS), an optical circulator, and an optical filter to reach a fiber-optic receiver, which would recover the RF signal and deliver it to other circuitry for further processing. The same optical fibers used to carry the modulated λ_1 signals to the center would also be used to carry a continuous-wave-RF-modulated calibration signal of wavelength λ_2 between the center and the antennas for use in stabilizing the phase of the λ_1 signals in the face of predominantly thermally induced fluctuations in the lengths of the optical fibers. The λ_2 calibration light returning to the center from each antenna would be separated from the λ_1 light by an optical filter and sent to another fiber-optic receiver, which would recover the con-

tinuous-wave RF calibration modulation. The RF output of this receiver would be compared with the original continuous-wave RF calibration modulation to obtain an error signal, which would be used as feedback to control the VOPS to compensate for any change in phase in propagation through the optical signal/calibration optical fiber and other optical components of the system. Additional optical fibers ($f_{13} \dots f_{N3}, f_{14} \dots f_{N4}$) would be used to carry the M/C signals. Inasmuch as the modulation on these signals would be at relatively low frequencies, there would be no need to stabilize them by use of VOPSs. This work was done by Shouhua Huang and Robert Tjoelker of Caltech for NASA's Jet Propulsion Laboratory. For more information, contact iaoffice@jpl.nasa.gov. NPO-44130

Reconfigurable, Bi-Directional Flexfet Level Shifter for Low-Power, Rad-Hard Integration

These level shifters enable the development of multi-level voltage systems.

Goddard Space Flight Center, Greenbelt, Maryland

Two prototype Reconfigurable, Bi-directional Flexfet Level Shifters (ReBiLS) have been developed, where one version is a stand-alone component designed to interface between external low voltage and high voltage, and the other version is an embedded integrated circuit (IC) for interface between internal low-voltage logic and external high-voltage components. Targeting stand-alone and embedded circuits separately allows optimization for these distinct applications. Both ReBiLS designs use the commercially available 180-nm Flexfet Independently Double-Gated (IDG) SOI CMOS (silicon on insulator, complementary metal oxide semiconductor) technology.

Embedded ReBiLS circuits were integrated with a Reed-Solomon (RS) encoder using CMOS Ultra-Low-Power Radiation Tolerant (CULPRiT) double-gated digital logic circuits. The scope of the project includes: creation of

a new high-voltage process, development of ReBiLS circuit designs, and adjustment of the designs to maximize performance through simulation, layout, and manufacture of prototypes.

The primary technical objectives were to develop a high-voltage, thick oxide option for the 180-nm Flexfet process, and to develop a stand-alone ReBiLS IC with two 8-channel I/O busses, 1.8–2.5 I/O on the low-voltage pins, 5.0-V-tolerant input and 3.3-V output I/O on the high-voltage pins, and 100-MHz minimum operation with 10-pF external loads.

Another objective was to develop an embedded, rad-hard ReBiLS I/O cell with 0.5-V low-voltage operation for interface with core logic, 5.0-V-tolerant input and 3.3-V output I/O pins, and 100-MHz minimum operation with 10-pF external loads.

A third objective was to develop a 0.5-V Reed-Solomon Encoder with embedded ReBiLS I/O:

- Transfer the existing CULPRiT RS encoder from a 0.35- μ m bulk-CMOS process to the ASI 180-nm Flexfet, rad-hard SOI Process.
- 0.5-V low-voltage core logic.
- 5.0-V-tolerant input and 3.3-V output I/O pins.
- 100-MHz minimum operation with 10-pF external loads.

The stand-alone ReBiLS chip will allow system designers to provide efficient bi-directional communication between components operating at different voltages. Embedding the ReBiLS cells into the proven Reed-Solomon encoder will demonstrate the ability to support new product development in a commercially viable, rad-hard, scalable 180-nm SOI CMOS process.

This work was done by Kelly DeGregorio and Dale G. Wilson of American Semiconductor, Inc. for Goddard Space Flight Center. Further information is contained in a TSP (see page 1). GSC-15565-1

Hardware-Efficient Monitoring of I/O Signals

Lyndon B. Johnson Space Center, Houston, Texas

In this invention, command and monitor functionality is moved between the two independent pieces of hardware, in which one had been dedicated to command and the other had been dedicated to monitor, such that some command and some monitor functionality appears in each. The only constraint is that the monitor for signal cannot be in the same hardware as the command I/O it is monitoring. The splitting of the command outputs between independent pieces of

hardware may require some communication between them, i.e. an intra-switch trunk line. This innovation reduces the amount of wasted hardware and allows the two independent pieces of hardware to be designed identically in order to save development costs.

This work was done by Kevin R. Driscoll, Brendan Hall, and Michael Paulitsch of Honeywell, Inc. for Johnson Space Center. For further information, contact the JSC Innovation Partnerships Office at (281) 483-3809.

Title to this invention has been waived under the provisions of the National Aeronautics and Space Act {42 U.S.C. 2457(f)} to Honeywell, Inc. Inquiries concerning licenses for its commercial development should be addressed to:

*Honeywell, Inc.
P.O. Box 52199
Phoenix, AZ 85072*

Refer to MSC-24458-1, volume and number of this NASA Tech Briefs issue, and the page number.

Video System for Viewing From a Remote or Windowless Cockpit

Lyndon B. Johnson Space Center, Houston, Texas

A system of electronic hardware and software synthesizes, in nearly real time, an image of a portion of a scene surveyed by as many as eight video cameras aimed, in different directions, at portions of the scene. This is a prototype of systems that would enable a pilot to view

the scene outside a remote or windowless cockpit. The outputs of the cameras are digitized.

Direct memory addressing is used to store the data of a few captured images in sequence, and the sequence is repeated in cycles. Cylindrical warp-

ing is used in merging adjacent images at their borders to construct a mosaic image of the scene. The mosaic-image data are written to a memory block from which they can be rendered on a head-mounted display (HMD) device. A subsystem in the

HMD device tracks the direction of gaze of the wearer, providing data that are used to select, for display, the portion of the mosaic image corresponding to the direction of gaze.

The basic functionality of the system has been demonstrated by mounting the cameras on the roof of a van and steering the van by use of the images presented on the HMD device.

This work was done by Amarnath Banerjee of Texas A&M University for Johnson Space Center. For further information, contact the JSC Innovation Partnerships Office at (281) 483-3809. MSC-23777-1

Spacesuit Data Display and Management System

John H. Glenn Research Center, Cleveland, Ohio

A prototype embedded avionics system has been designed for the next generation of NASA extra-vehicular-activity (EVA) spacesuits. The system performs biomedical and other sensor monitoring, image capture, data display, and data transmission. An existing NASA Phase I and II award winning design for an embedded computing system (ZIN vMetrics – BioWATCH) has been modified.

The unit has a reliable, compact form factor with flexible packaging options. These innovations are significant, because current state-of-the-art EVA spacesuits do not provide capability for data displays or embedded data acquisition and management. The Phase I effort achieved Technology Readiness Level 4 (high fidelity breadboard demonstration). The breadboard uses a commercial-grade field-programmable gate array (FPGA) with embedded

processor core that can be upgraded to a space-rated device for future revisions.

This work was done by David G. Hall, Aaron Sells, and Hemal Shah of ZIN Technologies, Inc. for Glenn Research Center.

Inquiries concerning rights for the commercial use of this invention should be addressed to NASA Glenn Research Center, Innovative Partnerships Office, Attn: Steve Fedor, Mail Stop 4-8, 21000 Brookpark Road, Cleveland, Ohio 44135. Refer to LEW-18399-1.

IEEE 1394 Hub With Fault Containment

Lyndon B. Johnson Space Center, Houston, Texas

This innovation is designed to prevent a single end system communication node from negatively influencing the whole system's behavior so that the network system can still operate if an end node is faulty. Placing a hub (star) in the middle of the system prevents propagation of critical control information that other end systems would react to, like block reset messages.

This work was done by Michael Paulitsch, Brendan Hall, and Kevin R. Driscoll of Honeywell, Inc. for Johnson Space Center. For further information, contact the JSC Innovation Partnerships Office at (281) 483-3809.

Title to this invention has been waived under the provisions of the National Aeronautics and Space Act {42 U.S.C. 2457(f)}

to Honeywell, Inc. Inquiries concerning licenses for its commercial development should be addressed to:

Honeywell, Inc.

P.O. Box 52199

Phoenix, AZ 85072

Refer to MSC-24459-1, volume and number of this NASA Tech Briefs issue, and the page number.

Compact, Miniature MMIC Receiver Modules for an MMIC Array Spectrograph

MMIC multi-chip modules can be used in astrophysics telescopes, automotive radar, and communication links.

NASA's Jet Propulsion Laboratory, Pasadena, California

A single-pixel prototype of a W-band detector module with a digital back-end was developed to serve as a building block for large focal-plane arrays of monolithic millimeter-wave integrated circuit (MMIC) detectors. The module uses low-noise amplifiers, diode-based mixers, and a WR10 waveguide input with a coaxial local oscillator. State-of-the-art InP HEMT (high electron mobility transistor) MMIC amplifiers at the front end provide approximately 40 dB of gain. The measured noise tempera-

ture of the module, at an ambient temperature of 300 K, was found to be as low as 450 K at 95 GHz.

The modules will be used to develop multiple instruments for astrophysics radio telescopes, both on the ground and in space. The prototype is being used by Stanford University to characterize noise performance at cryogenic temperatures. The goal is to achieve a 30–50 K noise temperature around 90 GHz when cooled to a 20 K ambient temperature. Further developments include

characterization of the IF in-phase (I) and quadrature (Q) signals as a function of frequency to check amplitude and phase; replacing the InP low-noise amplifiers with state-of-the-art 35-nm-gate-length NGC low-noise amplifiers; interfacing the front-end module with a digital back-end spectrometer; and developing a scheme for local oscillator and IF distribution in a future array.

While this MMIC is being developed for use in radio astronomy, it has the potential for use in other industries. Appli-

cations include automotive radar (both transmitters and receivers), communication links, radar systems for collision avoidance, production monitors, ground-penetrating sensors, and wireless personal networks.

This work was done by Pekka P. Kangaslahti, Todd C. Gaier, Joelle T. Cooperrider, Lorene A. Samoska, Mary M. Soria, Ian J. O'Dwyer, Sander Weinreb, Brian Custodero, and Heather Owen of Caltech; Keith Grainge of Cambridge University; Judy M. Lau and

Sarah Church of Stanford University; and Richard Lai and Xiaobing Mei of Northrop Grumman Corp. for NASA's Jet Propulsion Laboratory. Further information is contained in a TSP (see page 1). NPO-46522

Waveguide Transition for Submillimeter-Wave MMICs

NASA's Jet Propulsion Laboratory, Pasadena, California

An integrated waveguide-to-MMIC (monolithic microwave integrated circuit) chip operating in the 300-GHz range is designed to operate well on high-permittivity semiconductor substrates typical for an MMIC amplifier, and allows a wider MMIC substrate to be used, enabling integration with larger MMICs (power amplifiers). The waveguide-to-CBCPW (conductor-backed coplanar waveguide) transition topology is based on an integrated dipole placed in the E-plane of the waveguide module. It demonstrates low loss and good impedance matching. Measurement and simu-

lation demonstrate that the loss of the transition and waveguide loss is less than 1-dB over a 340-to-380-GHz bandwidth.

A transition is inserted along the propagation direction of the waveguide. This transition uses a planar dipole aligned with the maximum E-field of the TE₁₀ waveguide mode as an interface between the waveguide and the MMIC. Mode conversion between the coplanar striplines (CPS) that feed the dipole and the CBCPW transmission line is accomplished using a simple air-bridge structure. The bottom side ground plane is truncated at the same reference as the

top-side ground plane, leaving the end of the MMIC suspended in air.

This work was done by Kevin M. Leong, William R. Deal, Vesna Radisic, Xiaobing Mei, Jansen Uyeda, and Richard Lai of Northrop Grumman Corporation, and Lorene A. Samoska, King Man Fung, and Todd C. Gaier of Caltech for NASA's Jet Propulsion Laboratory. The work was sponsored under the DARPA SWIFT program and the contributors would like to acknowledge the support of Dr. Mark Rosker (DARPA) and Dr. H. Alfred Hung (Army Research Laboratory). Further information is contained in a TSP (see page 1). NPO-46237

Magnetic-Field-Tunable Superconducting Rectifier

This device would be useful in superconducting circuit applications.

Goddard Space Flight Center, Greenbelt, Maryland

Superconducting electronic components have been developed that provide current rectification that is tunable by design and with an externally applied magnetic field to the circuit component. The superconducting material used in the device is relatively free of pinning sites with its critical current determined by a geometric energy barrier to vortex entry. The ability of the vortices to move freely inside the device means this innovation does not suffer from magnetic hysteresis effects changing the state of the superconductor.

The invention requires a superconductor geometry with opposite edges along the direction of current flow. In order for the critical current asymmetry effect to

occur, the device must have different vortex nucleation conditions at opposite edges. Alternative embodiments producing the necessary conditions include edges being held at different temperatures, at different local magnetic fields, with different current-injection geometries, and structural differences between opposite edges causing changes in the size of the geometric energy barrier. An edge fabricated with indentations of the order of the coherence length will significantly lower the geometric energy barrier to vortex entry, meaning vortex passage across the device at lower currents causing resistive dissipation.

The existing prototype is a two-terminal device consisting of a thin-film su-

perconducting strip operating at a temperature below its superconducting transition temperature (T_c). Opposite ends of the strip are connected to electrical leads made of a higher T_c superconductor. The thin-film lithographic process provides an easy means to alter edge-structures, current-injection geometries, and magnetic-field conditions at the edges. The edge-field conditions can be altered by using local field(s) generated from dedicated higher T_c leads or even using the device's own higher T_c superconducting leads.

This work was done by John E. Sadleir of Goddard Space Flight Center. Further information is contained in a TSP (see page 1). GSC-15643-1



Bonded Invar Clip Removal Using Foil Heaters

Goddard Space Flight Center, Greenbelt, Maryland

A new process uses local heating and temperature monitoring to soften the adhesive under Invar clips enough that they can be removed without damaging the composite underneath or other nearby bonds. Two 1×1 in. ($\approx 2.5 \times 2.5$ cm), 10-W/in.² (≈ 1.6 W/cm²), 80-ohm resistive foil Kapton foil heaters, with pressure-sensitive

acrylic adhesive backing, are wired in parallel to a 50-V, 1-A limited power supply. At 1 A, 40 W are applied to the heater pair. The temperature is monitored in the clip radius and inside the tube, using a dual thermocouple readout. Several layers of aluminum foil are used to speed the heat up, allowing clips to be removed in less than five

minutes. The very local heating via the foil heaters allows good access for clip removal and protects all underlying and adjacent materials.

This work was done by James T. Pontius and James G. Tuttle of Goddard Space Flight Center. For further information, contact the Goddard Innovative Partnerships Office at (301) 286-5810. GSC-15770-1

Fabricating Radial Groove Gratings Using Projection Photolithography

Goddard Space Flight Center, Greenbelt, Maryland

Projection photolithography has been used as a fabrication method for radial groove gratings. Use of photolithographic method for diffraction grating fabrication represents the most significant breakthrough in grating technology in the last 60 years, since the introduction of holographic written gratings. Unlike traditional methods utilized for grating fabrication, this method has the advantage of producing complex diffractive groove contours that can be designed at pixel-by-pixel level, with pixel size currently at the level of 45×45 nm. Typical placement accuracy of the grating pixels is 10 nm over 30 nm. It is far superior to holographic, mechanically ruled or direct e-beam written gratings and results in high spatial coherence and low spectral cross-talk. Due to the smooth sur-

face produced by reactive ion etch, such gratings have a low level of randomly scattered light. Also, due to high fidelity and good surface roughness, this method is ideally suited for fabrication of radial groove gratings.

The projection mask is created using a laser writer. A single crystal silicon wafer is coated with photoresist, and then the projection mask, with its layer of photoresist, is exposed for patterning in a stepper or scanner. To develop the photoresist, the fabricator either removes the exposed areas (positive resist) of the unexposed areas (negative resist). Next, the patterned and developed photoresist silicon substrate is subjected to reactive ion etching. After this step, the substrate is cleaned. The projection mask is fabricated according to electronic design files

that may be generated in GDS file format using any suitable CAD (computer-aided design) or other software program.

Radial groove gratings in off-axis grazing angle of incidence mount are of special interest for x-ray spectroscopy, as they allow achieving higher spectral resolution for the same grating area and have lower alignment tolerances than traditional in-plane grating scheme. This is especially critical for NASA Constellation-X project that will utilize hundreds of gratings all of which need to be precisely aligned for x-ray observation of space.

This work was done by Dmitri Iazikov and Thomas W. Mossberg of LightSmyth Technologies for Goddard Space Flight Center. For further information, contact the Goddard Innovative Partnerships Office at (301) 286-5810. GSC-15686-1

Gratings Fabricated on Flat Surfaces and Reproduced on Non-Flat Substrates

This technology has application as diffraction gratings in optical components.

Goddard Space Flight Center, Greenbelt, Maryland

A method has been developed for fabricating gratings on flat substrates, and then reproducing the groove pattern on a curved (concave or convex) substrate and a corresponding grating device. First, surface relief diffraction grating grooves

are formed on flat substrates. For example, they may be fabricated using photolithography and reactive ion etching, maskless lithography, holography, or mechanical ruling. Then, an imprint of the grating is made on a deformable sub-

strate, such as plastic, polymer, or other materials using thermoforming, hot or cold embossing, or other methods. Interim stamps using electroforming, or other methods, may be produced for the imprinting process or if the same polarity

of the grating image is required. The imprinted, deformable substrate is then attached to a curved, rigid substrate using epoxy or other suitable adhesives. The imprinted surface is facing away from the curved rigid substrate.

As an alternative fabrication method, after grating is imprinted on the deformable substrate as described above, the grating may be coated with thin conformal conductive layer (for example, using vacuum deposition of gold). Then the membrane may be mounted over an opening in a pressured vessel in a manner of a membrane on a drum, grating side out. The pressure inside of the vessel may be changed with respect to the ambient pressure to produce concave or convex membrane surface. The shape of the opening may control the type of the surface curvature (for example, a circular opening would create spherical surface, oval opening would create toroidal surface, etc.). After that, well-known

electroforming methods may be used to create a replica of the grating on the concave or convex membrane. For example, the pressure vessel assembly may be submerged into an electro-forming solution and negative electric potential applied to the metal coated membrane using an insulated wire. Positive electric potential may be then applied to a nickel or other metal plate submerged into the same solution. Metal ions would transfer from the plate through the solution into the membrane, producing high fidelity metal replica of the grating on the membrane.

In one variation, an adhesive may be deposited on the deformable substrate, and then cured without touching the rigid, curved substrate. Edges of the deformable substrate may be attached to the rigid substrate to ensure uniform deformation of the deformable substrate. The assembly may be performed in vacuum, and then taken out to atmospheric

pressure conditions to ensure that no air is trapped between the deformable and rigid substrates.

Alternatively, a rigid surface with complementary curvature to the rigid substrate may be used to ensure uniform adhesion of the deformable substrate to the rigid substrate. Liquid may be applied to the surface of the deformable substrate to uniformly distribute pressure across its surface during the curing or hardening of the adhesive, or the film may be pressed into the surface using a deformable object or surface. After the attachment is complete, the grooves may be coated with reflective or dielectric layers to improve diffraction efficiency.

This work was done by David Content of Goddard Space Flight Center and Dmitri Iazikov, Thomas W. Mossberg, and Christopher M. Greiner of LightSmyth Technologies. Further information is contained in a TSP (see page 1). GSC-15769-1



Method for Measuring the Volume-Scattering Function of Water

Goddard Space Flight Center, Greenbelt, Maryland

The volume scattering function (VSF) of seawater affects visibility, remote sensing properties, in-water light propagation, lidar performance, and the like. Currently, it's possible to measure only small forward angles of VSF, or to use cumbersome, large, and non-autonomous systems. This innovation is a method of measuring the full range of VSF using a portable instrument.

A single rapid-sensing photosensor is used to scan a green laser beam, which

delivers the desired measurement. By using a single sensor, inter-calibration is avoided. A compact design is achieved by using drift-free detector electronics, fiber optics, and a new type of photomultiplier. This provides a high angular resolution of 1° or better, as well as the ability to focus in on a VSF region of particular interest.

Currently, the total scattering of light is measured as a difference from the other two parts of the light budget equa-

tion. This innovation will allow the direct calculation of the total scattering of light by taking an integral of the VSF over all angles. This directly provides one of the three components of the light budget equation, allowing greater versatility in its calculation.

This work was done by Yogesh C. Agrawal of Sequoia Scientific, Inc. for Goddard Space Flight Center. For further information, contact the Goddard Innovative Partnerships Office at (301) 286-5810. GSC-15395-1

Method of Heating a Foam-Based Catalyst Bed

John H. Glenn Research Center, Cleveland, Ohio

A method of heating a foam-based catalyst bed has been developed using silicon carbide as the catalyst support due to its readily accessible, high surface area that is oxidation-resistant and is electrically conductive. The foam support may be resistively heated by passing an electric current through it. This allows the catalyst bed to be heated directly, requiring less power to reach the desired temperature more quickly. Designed for heterogeneous catalysis, the method can be used by the petrochemical, chemical processing, and power-generating industries, as well as automotive catalytic converters.

Catalyst beds must be heated to a light-off temperature before they cat-

alyze the desired reactions. This typically is done by heating the assembly that contains the catalyst bed, which results in much of the power being wasted and/or lost to the surrounding environment. The catalyst bed is heated indirectly, thus requiring excessive power. With the electrically heated catalyst bed, virtually all of the power is used to heat the support, and only a small fraction is lost to the surroundings.

Although the light-off temperature of most catalysts is only a few hundred degrees Celsius, the electrically heated foam is able to achieve temperatures of 1,200 °C. Lower temperatures are achievable by supplying less electrical power to

the foam. Furthermore, because of the foam's open-cell structure, the catalyst can be applied either directly to the foam ligaments or in the form of a catalyst-containing washcoat. This innovation would be very useful for heterogeneous catalysis where elevated temperatures are needed to drive the reaction.

This work was done by Arthur J. Fortini, Brian E. Williams, and Shawn R. McNeal of Ultramet for John Glenn Research Center.

Inquiries concerning rights for the commercial use of this invention should be addressed to NASA Glenn Research Center, Innovative Partnerships Office, Attn: Steve Fedor, Mail Stop 4-8, 21000 Brookpark Road, Cleveland, Ohio 44135. Refer to LEW-18155-1.

Small Deflection Energy Analyzer for Energy and Angular Distributions

NASA's Goddard Space Flight Center, Greenbelt, Maryland

The development of the Small Deflection Energy Analyzer (SDEA) charged-particle spectrometer for energy and angle distributions responds to a long-standing need to measure the wind velocity vector in Earth's thermosphere, and to obtain the ion-drift vector in the ionosphere. The air and ions above 120 km are endowed with bulk velocities and tem-

peratures just like air near the ground, but with separate spatial and temporal variations. It is important to understand these not only for study of the physics and chemistry of the Sun-Earth connection, but also for spacecraft orbit predictions, and communications through the ionosphere.

The SDEA consists of a pair of parallel conducting plates separated by a small

distance, with an entrance slit on one end, and an exit slit on the other. A voltage applied to these plates develops an electric field between the plates, and this field deflects ions passing through it. If an ion has too little energy, it will strike one of the plates. If it has too much, it will strike the back wall. An ion with the amount of energy being searched for

will have its trajectory bent just enough to exit the back slit.

The SDEA units are compact, rectangular, and operate with low voltages. The units can be built up into small arrays. These arrays could be used either to widen the field of view or to sharpen an

existing one. This approach can also be used to obtain angular distributions in two planes simultaneously, thus cutting down the ion source power requirements in half. This geometry has enabled a new mass-spectrometer concept that can provide miniaturized mass spectrometers for

use in industrial plants, air-pollution monitoring, and noxious-gas detection.

This work was done by Federico A. Herrero of Goddard Space Flight Center. For further information, contact the Goddard Innovative Partnerships Office at (301) 286-5810. GSC-15610-1

Polymeric Bladder for Storing Liquid Oxygen

Lyndon B. Johnson Space Center, Houston, Texas

A proposed system for storing oxygen in liquid form and dispensing it in gaseous form is based on (1) initial subcooling of the liquid oxygen; (2) containing the liquid oxygen in a flexible vessel; (3) applying a gas spring to the flexible vessel to keep the oxygen compressed above the saturation pressure and, thus, in the liquid state; and (4) using heat leakage into the system for vaporizing the oxygen to be dispensed. In a typical prior system based on these principles, the flexible vessel

is a metal bellows housed in a rigid tank, and the gas spring consists of pressurized helium in the tank volume surrounding the bellows. Unfortunately, the welds in the bellows corrugations are subject to fatigue, and, because bellows have large ullage, a correspondingly large fraction of the oxygen content cannot be expelled.

In the proposed system, the flexible vessel would be a bladder made of a liquid-crystal polymer (LCP). (LCPs are strong and compatible with liquid oxy-

gen.) In comparison with a metal bellows, a polymeric bladder would have less ullage and would weigh less. In experiments involving fatigue cycling at liquid-nitrogen temperatures, two LCPs were found to be suitable for this application.

This work was done by David H. Walker, Andrew C. Harvey, and William Leary of Foster-Miller, Inc. for Johnson Space Center. For further information, contact the JSC Innovation Partnerships Office at (281) 483-3809. MSC-22943-1

Pyrotechnic Simulator/Stray-Voltage Detector

John F. Kennedy Space Center, Florida

The concept for a dual test item has been developed for use in simulating live initiators/detonators during ground testing to verify the proper operation of the safing and firing circuitry for ground and flight systems ordnance as well as continuous monitoring for any stray voltages. Previous ordnance simulators have consisted of fuses, flash bulbs, inert

devices with bridge wires, and actual live ordnance items mounted in test chambers. Stray voltage detectors have included devices connected to the firing circuits for continuous monitoring and a final no-voltage test just prior to ordnance connection. The purpose of this combined ordnance simulation and stray-voltage detection is to provide an

improved and comprehensive method to ensure the ordnance circuitry is verified safe and operational.

This work was done by Terry Greenfield of ASRC Aerospace Corp. for Kennedy Space Center. For further information, contact the Kennedy Innovative Partnerships Program Office at (321) 861-7158. KSC-13282

Inventions Utilizing Microfluidics and Colloidal Particles

Lyndon B. Johnson Space Center, Houston, Texas

Several related inventions pertain to families of devices that utilize microfluidics and/or colloidal particles to obtain useful physical effects. The families of devices can be summarized as follows:

- Microfluidic pumps and/or valves wherein colloidal-size particles driven by electrical, magnetic, or optical fields serve as the principal moving parts that propel and/or direct the affected flows.
- Devices that are similar to the aforementioned pumps and/or valves ex-

cept that they are used to manipulate light instead of fluids. The colloidal particles in these devices are substantially constrained to move in a plane and are driven to spatially order them into arrays that function, variously, as waveguides, filters, or switches for optical signals.

- Devices wherein the ultra-laminar nature of microfluidic flows is exploited to effect separation, sorting, or filtering of colloidal particles or biological cells in suspension.

- Devices wherein a combination of confinement and applied electrical and/or optical fields forces the colloidal particles to become arranged into three-dimensional crystal lattices. Control of the colloidal crystalline structures could be exploited to control diffraction of light.
- Microfluidic devices, incorporating fluid waveguides, wherein switching of flows among different paths would be accompanied by switching of optical signals.

This work was done by David W. M. Marr, Tieying Gong, John Oakey, Alexander V. Ter-ray, and David T. Wu of the Colorado School of Mines for Johnson Space Center. Further information is contained in a TSP (see page 1).

In accordance with Public Law 96-517, the contractor has elected to retain title to this invention. Inquiries concerning rights for its commercial use should be addressed to:

*Colorado School of Mines
Golden, CO 80401
Refer to MSC-24160-1/1-1/2-1/3-1, volume and number of this NASA Tech Briefs issue, and the page number.*

RuO₂ Thermometer for Ultra-Low Temperatures

Goddard Space Flight Center, Greenbelt, Maryland

A small, high-resolution, low-power thermometer has been developed for use in ultra-low temperatures that uses multiple RuO₂ chip resistors. The use of commercially available thick-film RuO₂ chip resistors for measuring cryogenic temperatures is well known due to their low cost, long-term stability, and large resistance change.

To measure the resistance, a small excitation is applied across the sensor and the resistance is measured. At increased currents, a greater output signal is achieved, resulting in better sensitivity.

Problems including lowered resolution and sensitivity are found because of self-heating at temperatures below 100 mK when a single chip is used.

A new thermometer design uses multiple RuO₂ chip resistors and off-the-shelf bobbins. The chips would be configured in an array to spread the heat over a greater area during excitation. A technique was developed to connect the chips together, first in a 2×2 array, and finally in a 3×3 array. The 3×3 array configuration of the RuO₂ chips allows better internal heat distribution than a

single chip, thereby reducing self-heating. The uniqueness of this design is in the array configuration, which allows greater sensitivity at ultralow temperatures while keeping a small package footprint [about 0.4 in. (10 mm)]. The device uses a standard round bobbin with a #4 screw through-hole.

This work was done by Thomas Hait, Peter J. Shirron, and Michael DiPirro of Goddard Space Flight Center. For further information, contact the Goddard Innovative Partnerships Office at (301) 286-5810. GSC-15690-1

Ultra-Compact, High-Resolution LADAR System for 3D Imaging

Lyndon B. Johnson Space Center, Houston, Texas

An eye-safe LADAR system weighs under 500 grams and has range resolution of 1 mm at 10 m. This laser uses an adjustable, tiny microelectromechanical system (MEMS) mirror that was made in SiWave to sweep laser frequency. The size of the laser device is small (70×50×13 mm). The LADAR uses all the mature fiber-optic telecommunication technologies in the system, making this innovation an efficient performer. The tiny size and

light weight makes the system useful for commercial and industrial applications including surface damage inspections, range measurements, and 3D imaging.

This work was done by Jing Xu and Roman Gutierrez of SiWave, Inc. for NASA's Johnson Space Center. For further information, contact the JSC Innovation Partnerships Office at (281) 483-3809.

In accordance with Public Law 96-517, the contractor has elected to retain title to this

invention. Inquiries concerning rights for its commercial use should be addressed to:

*SiWave
400 East Live Oak Avenue
Arcadia, CA 91006-5619
Phone No.: (626) 821-0570
Fax No.: (626) 446-7259
E-mail: www.siwaveinc.com
Refer to MSC-23873-1, volume and number of this NASA Tech Briefs issue, and the page number.*

Dual-Channel Multi-Purpose Telescope

Goddard Space Flight Center, Greenbelt, Maryland

A dual-channel telescope allows for a wide-field telescope design with a good, narrow field channel of fewer surfaces for shorter-wavelength or planet-finding applications. The design starts with a Korsch three-mirror-anastigmat (TMA) telescope that meets the mission criteria for image quality over a wide field of view. The internal image at the Cassegrain focus is typically blurry due to the aberration balancing among the three mirrors. The

Cassegrain focus is then re-optimized on the axis of the system where the narrow field channel instrument is picked off by bending the primary mirror. This now makes the wide-field channel blurry (i.e., the TMA image), and it must be re-optimized while holding the fore-optics fixed. This leaves the tertiary mirror as a variable, as well as a fold mirror strategically placed at the image of the primary mirror (i.e., exit pupil of the telescope). This fold

mirror can then be used to compensate for the departure in primary mirror figure used to optimize the narrow field channel. As such, only an aspheric term is needed for this final optimization on this "corrector" fold mirror.

This work was done by Joseph M. Howard and David Content of Goddard Space Flight Center. For further information, contact the Goddard Innovative Partnerships Office at (301) 286-5810. GSC-15574-1

Objective Lens Optimized for Wavefront Delivery, Pupil Imaging, and Pupil Ghosting

Goddard Space Flight Center, Greenbelt, Maryland

An interferometer objective lens (or diverger) may be used to transform a collimated beam into a diverging or converging beam. A typical objective lens is optimized to deliver a diffraction-limited beam to an optic or optical system under test. Often, imaging performance with respect to the interferometer pupil is not optimal. The center of curvature test for the James Webb Space Telescope required a better solution.

This innovation provides an objective lens that has diffraction-limited optical performance that is optimized at two sets of conjugates: imaging to the objective focus and imaging to the pupil. The

lens thus provides for simultaneous delivery of a high-quality beam and excellent pupil resolution properties.

A typical objective lens can also introduce objectionable back reflections (or ghosts) into the interferometer, which can produce visible interference rings. This interference degrades, and can even mask, the quality of the measurements being made. The new lens eliminates this common problem. For each surface in the objective lens, the absolute value angle of incidence of the marginal rays is maintained above a minimal threshold for beam delivery. Angle of incidence control has the effect of

producing highly divergent and out-of-focus reflections with low intensities at the entrance to the interferometer. The results are minimized ghosting and improved data quality.

This objective lens is suitable for any kind of testing or sensing using an interferometer when high spatial resolution is required, and is especially well suited for tests that include segmented optical components or large apertures.

This work was done by Gene Olczak of ITT Space Systems Division, LLC for Goddard Space Flight Center. For further information, contact the Goddard Innovative Partnerships Office at (301) 286-5810. GSC-15675-1

CMOS Camera Array With Onboard Memory

Goddard Space Flight Center, Greenbelt, Maryland

A compact CMOS (complementary metal oxide semiconductor) camera system has been developed with high resolution (1.3 Megapixels), a USB (universal serial bus) 2.0 interface, and an onboard memory. A compact design of a 2×4 in. (≈5×10 cm) multilayer PCB (printed circuit board) was designed that contains the CMOS socket, a PLD (programmable logic device) for the digital logic required to drive the CMOS array, the USB 2.0 interface, and a RAM (random access memory) chip for storing up to nine images in a compact format. The system can

be configured as a slave, which allows the camera to receive a trigger from another similar camera to synchronize exposure, or in master mode, in which the camera receives a trigger command from a computer and sends a trigger to other cameras for synchronization.

Exposure times, and other operating parameters, are sent from a control PC via the USB port. Data from the camera can be received via the USB port and the interface allows for simple control and data capture through a laptop computer. The software designed for this sys-

tem manages synchronized image capture as used in Pentacam with CMOS sensors, and no frame-grabbers so the power consumption is minimal.

Since the cameras can be triggered and synchronized, they can be used to capture images of high-speed events from several directions. Remote sensing applications also can take advantage of these systems.

This work was done by Nahum Gat of Opto-Knowledge Systems, Inc. for Goddard Space Flight Center. For further information, contact the Goddard Innovative Partnerships Office at (301) 286-5810. GSC-14902-1



Quickly Approximating the Distance Between Two Objects

Lyndon B. Johnson Space Center, Houston, Texas

A method of quickly approximating the distance between two objects (one smaller, regarded as a point; the other larger and complexly shaped) has been devised for use in computationally simulating motions of the objects for the purpose of planning the motions to prevent collisions. The method is needed because computer-based-graphics techniques that have been used heretofore to make such estimates entail amounts of computation that are excessively large for purposes of the simulations.

The method, denoted tree-based model learning, is an integral combination of (1) decision-tree techniques upon which several machine learning techniques have been based and (2) a relatively accurate function-approximation technique. Each node of a decision tree corresponds to a partition of the problem domain — in this case, starting with one node representing a large cubic volume centered on the large object and dividing and subdividing it, at symmetry planes, into suc-

cessively smaller cubes. Each branch of the tree represents a rule-based decision selecting one of the child nodes of a parent node. The smallest subdivisions (leaf nodes) contain coefficients of a quadric equation that estimates the distance between the objects.

This work was done by David Hammen of LinCom Corp. for Johnson Space Center. For further information, contact the JSC Innovation Partnerships Office at (281) 483-3809. MSC-23264-1

Processing Images of Craters for Spacecraft Navigation

NASA's Jet Propulsion Laboratory, Pasadena, California

A crater-detection algorithm has been conceived to enable automation of what, heretofore, have been manual processes for utilizing images of craters on a celestial body as landmarks for navigating a spacecraft flying near or landing on that body. The images are acquired by an electronic camera aboard the spacecraft, then digitized, then processed by the algorithm, which consists mainly of the following steps:

1. Edges in an image detected and placed in a database.

2. Crater rim edges are selected from the edge database.
3. Edges that belong to the same crater are grouped together.
4. An ellipse is fitted to each group of crater edges.
5. Ellipses are refined directly in the image domain to reduce errors introduced in the detection of edges and fitting of ellipses.
6. The quality of each detected crater is evaluated.

It is planned to utilize this algorithm

as the basis of a computer program for automated, real-time, onboard processing of crater-image data. Experimental studies have led to the conclusion that this algorithm is capable of a detection rate >93 percent, a false-alarm rate <5 percent, a geometric error <0.5 pixel, and a position error <0.3 pixel.

This work was done by Yang Cheng, Andrew E. Johnson, and Larry H. Matthies of Caltech for NASA's Jet Propulsion Laboratory. For more information, contact iaoffice@jpl.nasa.gov. NPO-40122

Adaptive Morphological Feature-Based Object Classifier for a Color Imaging System

This technique has potential use in the fields of disease state identification, cancer screening and detection, and wound healing.

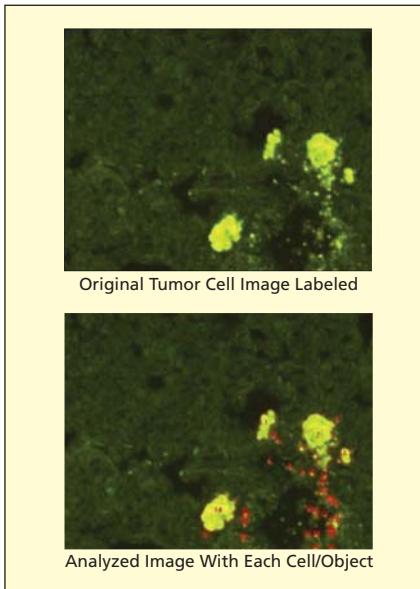
John H. Glenn Research Center, Cleveland, Ohio

Utilizing a Compact Color Microscope Imaging System (CCMIS), a unique algorithm has been developed that combines human intelligence along with machine vision techniques to produce an autonomous microscope tool for biomedical, industrial, and space applications. This technique is based on an adaptive, morphological,

feature-based mapping function comprising 24 mutually inclusive feature metrics that are used to determine the metrics for complex cell/objects derived from color image analysis. Some of the features include:

- Area (total numbers of non-background pixels inside and including the perimeter),

- Bounding Box (smallest rectangle that bounds and object),
- centerX (*x*-coordinate of intensity-weighted, center-of-mass of an entire object or multi-object blob),
- centerY (*y*-coordinate of intensity-weighted, center-of-mass, of an entire object or multi-object blob),
- Circumference (a measure of circumfer-



CCMIS Automatically Identifies Tumor Morphology of florescence stained images. The key with this application is that the second set of tumor images above could not be identified by human experts. However, CCMIS was able to identify the tumor cells in seconds.

ence that takes into account whether neighboring pixels are diagonal, which is a longer distance than horizontally or vertically joined pixels),

- Elongation (measure of particle elongation given as a number between 0 and 1. If equal to 1, the particle bounding box is square. As the elongation decreases from 1, the particle becomes more elongated),
- Ext_vector (extremal vector),
- Major Axis (the length of a major axis of a smallest ellipse encompassing an object),
- Minor Axis (the length of a minor axis of a smallest ellipse encompassing an object),
- Partial (indicates if the particle extends beyond the field of view),
- Perimeter Points (points that make up a particle perimeter),
- Roundness [$(4\pi \times \text{area}) / \text{perimeter}^2$] the result is a measure of object roundness, or compactness, given as a value between 0 and 1. The greater the ratio, the rounder the object.],

- Thin in center (determines if an object becomes thin in the center, (figure-eight-shaped),
- Theta (orientation of the major axis),
- Smoothness and color metrics for each component (red, green, blue) the minimum, maximum, average, and standard deviation within the particle are tracked.

These metrics can be used for autonomous analysis of color images from a microscope, video camera, or digital, still image. It can also automatically identify tumor morphology of stained images and has been used to detect stained cell phenomena (see figure).

This work was done by Mark McDowell of Glenn Research Center and Elizabeth Gray of Scientific Consulting, Inc. Further information is contained in a TSP (see page 1).

Inquiries concerning rights for the commercial use of this invention should be addressed to NASA Glenn Research Center, Innovative Partnerships Office, Attn: Steve Fedor, Mail Stop 4-8, 21000 Brookpark Road, Cleveland, Ohio 44135. Refer to LEW-18291-1.

🔍 Rover Slip Validation and Prediction Algorithm

NASA's Jet Propulsion Laboratory, Pasadena, California

A physical-based simulation has been developed for the Mars Exploration Rover (MER) mission that applies a slope-induced wheel-slippage to the rover location estimator. Using the digital elevation map from the stereo images, the computational method resolves the quasi-dynamic equations of motion that incorporate the actual wheel-terrain speed to estimate the gross velocity of the vehicle.

Based on the empirical slippage measured by the Visual Odometry software of the rover, this algorithm computes two factors for the slip model by minimizing the distance of the predicted and actual vehicle location, and then uses the model to predict the next drives. This technique, which has been deployed to operate the MER rovers in the extended mission periods, can accurately predict the rover position and

attitude, mitigating the risk and uncertainties in the path planning on high-slope areas.

This work was done by Jeng Yen of Caltech for NASA's Jet Propulsion Laboratory.

The software used in this innovation is available for commercial licensing. Please contact Karina Edmonds of the California Institute of Technology at (626) 395-2322. Refer to NPO-45240.

🔍 Safety and Quality Training Simulator

Lyndon B. Johnson Space Center, Houston, Texas

A portable system of electromechanical and electronic hardware and documentation has been developed as an automated means of instructing technicians in matters of safety and quality. The system enables elimination of most of the administrative tasks associated with traditional training. Customized, performance-based, hands-on training with integral testing is substituted for the traditional instructional ap-

proach of passive attendance in class followed by written examination.

The system includes four workstations, accommodating up to eight students. The system simulates hazardous conditions (without exposing students to real hazards) and quality or safety discrepancies that students are required to recognize and for which the students are required to perform corrective actions. The system enables students to demon-

strate knowledge gained from previous training and work experience. The system provides remedial training for each student who does not perform satisfactorily in a simulation.

This work was done by Pete T. Scobby of United Space Alliance for Johnson Space Center. Further information is contained in a TSP (see page 1). MSC-23232-1

Supply-Chain Optimization Template

Lyndon B. Johnson Space Center, Houston, Texas

The Supply-Chain Optimization Template (SCOT) is an instructional guide for identifying, evaluating, and optimizing (including re-engineering) aerospace-oriented supply chains. The SCOT was derived from the Supply Chain Council's Supply-Chain Operations Reference (SCC SCOR) Model, which is more generic and more oriented toward achieving a competitive advantage in business.

Utilizing NASA's Parachute Refurbishment Facility as an example, concepts

contained in the SCC SCOR Model were modified and expanded to be applicable to the unique processes, restrictions, and regulations found in aerospace environments. Templates of the optimized processes were created, samples were developed, and validated effective processes of implementation were created. These templates, samples, and processes were integrated into a formal step-by-step set of descriptions of only those processes applicable in aerospace settings. The inclusion of these specific

process steps, coupled with the exclusion of generic SCC SCOR Model process steps that are not applicable in aerospace settings, is expected to reduce the amounts of time needed to both optimize supply chains and train personnel to optimize supply chains.

This work was done by William F. Quiett and Scott L. Sealing of United Space Alliance for Johnson Space Center. Further information is contained in a TSP (see page 1). MSC-23423-1

Algorithm for Computing Particle/Surface Interactions

Goddard Space Flight Center, Greenbelt, Maryland

An algorithm has been devised for predicting the behaviors of sparsely spatially distributed particles impinging on a solid surface in a rarefied atmosphere. Under the stated conditions, prior particle-transport models in which (1) dense distributions of particles are treated as continuum fluids; or (2) sparse distributions of particles are considered to be

suspended in and to diffuse through fluid streams are not valid.

In the present algorithm, individual particle/surface interactions are modeled. The algorithm uses a few key parameters that can be determined experimentally for the particles of interest in a given application: These parameters are the coefficient of restitution, coefficient of trans-

fer of momentum, diffusivity, and sticking velocity. If many representative particles are tracked through modeling by use of this algorithm, a statistically likely distribution of particles can be obtained.

This work was done by David W. Hughes of Goddard Space Flight Center. Further information is contained in a TSP (see page 1). GSC-15364-1



Cryogenic Pupil Alignment Test Architecture for Aber-rated Pupil Images

A document describes cryogenic test architecture for the James Webb Space Telescope (JWST) integrated science instrument module (ISIM). The ISIM element primarily consists of a mechanical metering structure, three science instruments, and a fine guidance sensor. One of the critical optomechanical alignments is the co-registration of the optical telescope element (OTE) exit pupil with the entrance pupils of the ISIM instruments. The test architecture has been developed to verify that the ISIM element will be properly aligned with the nominal OTE exit pupil when the two elements come together.

The architecture measures three of the most critical pupil degrees-of-freedom during optical testing of the ISIM element. The pupil measurement scheme makes use of specularly reflective pupil alignment references located inside the JWST instruments, ground support equipment that contains a pupil imaging module, an OTE simulator, and pupil viewing channels in two of the JWST flight instruments.

Pupil alignment references (PARs) are introduced into the instrument, and their reflections are checked using the instrument's mirrors. After the pupil imaging module (PIM) captures a reflected PAR image, the image will be analyzed to determine the relative alignment offset. The instrument pupil alignment preferences are specularly reflective mirrors with non-reflective fiducials, which makes the test architecture feasible. The instrument channels have fairly large fields of view, allowing PAR tip/tilt tolerances on the order of 0.5° .

This work was done by Brent Bos, David A. Kubalak, Scott Antonille, Raymond Ohl, and John G. Hagopian of Goddard Space Flight Center. Further information is contained in a TSP (see page 1). GSC-15650-1

Thermal Transport Model for Heat Sink Design

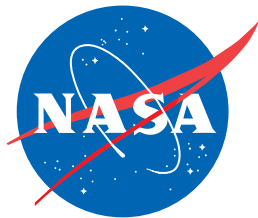
A document discusses the development of a finite element model for describing thermal transport through microcalorimeter arrays in order to assist in heat-sinking design. A fabricated multiabsorber transition edge sensor (PoST) was designed in order to reduce device wiring density by a factor of four.

The finite element model consists of

breaking the microcalorimeter array into separate elements, including the transition edge sensor (TES) and the silicon substrate on which the sensor is deposited. Each element is then broken up into subelements, whose surface area subtends 10×10 microns. The heat capacity per unit temperature, thermal conductance, and thermal diffusivity of each subelement are the model inputs, as are the temperatures of each subelement. Numerical integration using the Finite in Time Centered in Space algorithm of the thermal diffusion equation is then performed in order to obtain a temporal evolution of the subelement temperature. Thermal transport across interfaces is modeled using a thermal boundary resistance obtained using the acoustic mismatch model.

The document concludes with a discussion of the PoST fabrication. PoSTs are novel because they enable incident x-ray position sensitivity with good energy resolution and low wiring density.

This work was done by James A. Chervenak, Richard L. Kelley, Ari D. Brown, Stephen J. Smith, and Caroline A. Kilbourne of Goddard Space Flight Center. Further information is contained in a TSP (see page 1). GSC-15671-1



National Aeronautics and
Space Administration